

# Multiple time scales in a strongly coupled dusty plasma revealed by survival-function analysis

Chun-Shang Wong,<sup>\*</sup> J. Goree, and Zach Haralson<sup>†</sup>

*Department of Physics and Astronomy, The University of Iowa, Iowa City, Iowa 52242, USA*

(Dated: October 16, 2018)

Under liquid-like conditions, particles are found to rearrange on multiple time scales in a two-dimensional dusty plasma experiment. Our analysis is based on survival functions, which are time-series graphs of the probability that a particle's number of nearest neighbors remains unchanged. Non-defects are found to exhibit two distinct time scales, revealed by an elbow in their survival function. Defects have survival functions that are more nearly exponential, with decay rates that offer insight at a microscopic level into the viscoelastic relaxation in a liquid.

*Introduction.*—Strongly coupled plasmas can often behave like liquids [1–6]. Among all kinds of strongly coupled plasmas, one that can be studied most easily in laboratory experiments is a dusty plasma [7–16]. A dusty plasma is a four-component mixture of micron-sized solid particles, ions, electrons, and neutral gas atoms. The solid particles gain large negative electric charges, so that the ensemble of particles is strongly coupled, with an interparticle potential energy that exceeds their kinetic energy. The particles self-organize with a microstructure that is liquid-like when laser heating is applied [17]. Direct imaging [18] and tracking [19] of individual particles enables an experimental study of microscopic dynamics.

Previous studies of strongly coupled plasmas have often centered on the concept of relaxation [20–30], and in particular, a relaxation time. Dating back to Maxwell [31], this description of liquids is a microscopic model that characterizes interparticle interactions as a viscoelastic combination of elasticity and dissipation, which dominate at short and long times, respectively. However, we suggest that the relaxation time can be an oversimplification, because as a single-value measure, it cannot reflect the full complexity of a liquid's spatial and temporal dynamics.

In this Rapid Communication, we seek a more detailed description of the microscopic rearrangements in a strongly coupled plasma by using a time-series curve called a survival function. This approach improves upon the use of a single-value measure like the relaxation time, and it allows us to detect a previously unreported complexity: two distinct time scales in the microscopic evolution for non-defects. Defects, in contrast to non-defects, evolve with a nearly exponential decay with a faster rate, which varies with temperature and the type of defect.

A survival function [32] is a graph of the probability that an entity or condition remains unchanged after a specified time [33]. Survival functions are used, for example, in medicine, where a human's probability of remaining alive can be plotted versus time, beginning when a cancer is diagnosed [34]. In engineering, the probability that a solid object under stress remains intact [35] can be plotted as a survival function. In nuclear physics, a

radioactive decay graph is another example of a survival function. Like all survival functions, these curves begin at 100% and gradually diminishes with time.

The shape of a survival function can offer insight into underlying processes. For example, in nuclear physics, the shape is exponential, reflecting the stochastic nature of nuclear decay. In demography, on the other hand, the survival function of a wealthy country's population has a shape that is nearly flat from birth until about 65 years, after which there is a large drop [36], reflecting how a human body ages.

Preparing a survival function, in general, requires tracking an entity or condition that can change, such as radioactivity or human lives. In this Rapid Communication, the condition we track is coordination.

Coordination (also called coordination number) is an instantaneous count of a particle's nearest neighbors [37, 38]. This microscopic measure of structure is a familiar tool of chemistry and material physics, and it has also been applied to liquids [39–42] and strongly coupled plasmas [27, 43, 44].

A particle is classified as either a *defect* or a *non-defect* according the local microstructure [37]. In 2D, if a particle's coordination is six-fold, then the microstructure is non-defective, which is the case everywhere in a perfect crystal. On the other hand, a defect is any coordination that is not six-fold [45]. We will use the term “all defects” to include the common five- and seven-fold defects, as well as the less common four- and eight-fold defects. Only a slight displacement of particles is required to convert a non-defect into a defect, and vice versa. Defects, which are expected to be unstable, are eliminated constantly from a liquid. Of course, in a steady state, new defects must be created to balance those that are eliminated.

Coordination was found to be useful in obtaining a connectivity time for simulations of simple liquids [41], liquid metals [42], and strongly coupled dusty plasmas [27]. Such a connectivity time serves a single-value measurement of relaxation, which has been used for example to gain physical intuition into the microscopic origins of shear relaxation [27]. However, as a single-value mea-

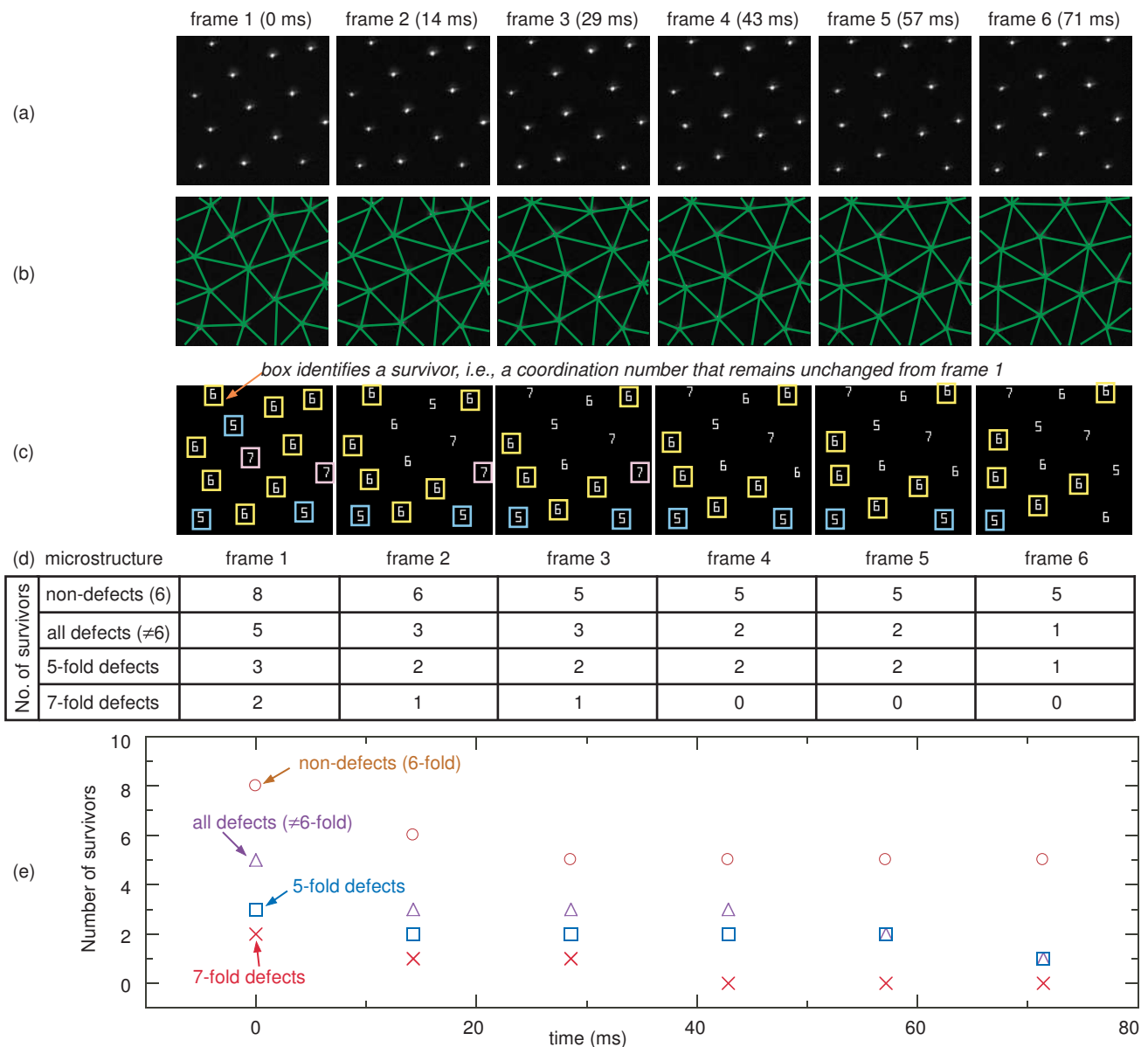


FIG. 1. (color online). Illustrative example of our analysis method. (a) Images of consecutive video frames, which allow measurements of particle positions. (b) Delaunay triangulation is applied to identify nearest neighbors, which are joined by the drawn line segments. The number of line segments originating at the location of a particle is its coordination. (c) Particle coordination maps are obtained by recording the coordination value of each particle at its position. Next, we track particles and their coordinations from frame to frame, and identify the event when its coordination first changes. Until this event, that coordination is considered to be a survivor, as identified by the outlining boxes. In each frame, we count the number of five-fold coordinations (likewise for six and seven-fold coordination) that have survived since the initial frame. The resulting table of data (d) is plotted in (e) as a time series, which are the survival functions. The images here were cropped for brevity; their area is 1% of the camera’s full field of view.

sure, connectivity time has the shortcoming we mentioned above, that it cannot capture a complex temporal evolution. Moreover, it also discards the distinction between defects and non-defects.

Our analysis method includes three advances in the use of coordination to characterize relaxation. First, we distill our structural measurements not into a single-value measure but into a richer description presented as a sur-

vival function. Second, we analyze coordination data separately for defects and non-defects. Third, we base our analysis on a more rigorous measure of coordination using Delaunay triangulation. With these advances, we are able to make the discovery, presented below, that non-defects evolve with two time scales.

*Experiment.*—Data from the 2D strongly coupled dusty plasma experiment of Haralson *et al.* [46, 47]

are further analyzed here. This experiment, which was originally performed to study other aspects of liquid physics [30, 47], is also well suited for our analysis. About  $10^4$  polymer microspheres of  $8.69 \mu\text{m}$  diameter were introduced into a radio-frequency discharge using argon at 6 mTorr. Particles had a charge of  $-15\,500e$ . The particles were levitated in a single horizontal layer, and with a strong coupling so great that they initially self-organized into a crystalline triangular lattice structure [48–52]. For each experimental run, this lattice was melted using laser heating to increase the particle kinetic energies [17]. The laser-heated ensemble of particles was confirmed to exhibit steady-state liquid-like behavior.

We analyze eight experimental runs. They had similar conditions except for different kinetic temperatures  $T$  of the particles, ranging from  $T = 96\,800\text{ K}$  to  $127\,000\text{ K}$ ; the corresponding Coulomb coupling parameters ranged from  $\Gamma = 139$  to  $104$ . Other parameters for the experimental run analyzed in detail in this Rapid Communication include: Einstein frequency [53]  $\Omega_E = 50.2\text{ s}^{-1}$ , nominal 2D dust plasma frequency  $\omega_{\text{pd}} = 86\text{ s}^{-1}$ , frictional damping rate due to gas  $1.1\text{ s}^{-1}$ , particle spacing characterized by the Wigner-Seitz radius  $a = 0.30\text{ mm}$ , and screening parameter  $\kappa = a/\lambda = 0.72$ , where  $\lambda$  is the screening length.

The primary diagnostic was video microscopy, using a top-view camera imaging at 70 frames/s. Examples images are shown in Fig. 1(a). Analysis of images, using the moment method, yielded particle positions with sub-pixel precision, in each video frame. Further details of the experiment are provided in Refs. [46, 47].

*Delaunay-based particle coordination.*—Our structural analysis of the particle position data in a single video frame requires identifying nearest neighbors. We use Delaunay triangulation, which is a rigorous geometrical analysis method that accounts for not only the distances between particles, but also their arrangement [44]. In Delaunay triangulation, Fig. 1(b), a particle is represented by a vertex, which connects line segments that we count to obtain the coordination. A coordination map, as in Fig. 1(c), corresponds to a single video frame. We prepare a sequence of these coordination maps to observe the temporal development. In a liquid, the coordination for a given particle does not remain static, but evolves [54] as can be seen in the sequence of coordination maps in Fig. 1(c), and in the video provided in the Supplemental Material [55].

The Delaunay approach improves upon a common method of obtaining the coordination values that was used to measure connectivity times for liquids [27, 38, 41, 42]. In that method, a specified search radius is used in counting the nearest neighbors. The resulting count depends on how the search radius is defined. We instead count the nearest neighbors identified by Delaunay triangulation, which has no adjustable parameters [56].

*Survival-function analysis method.*—A starting time is

selected as one frame of the video. In this frame, we identify the coordination of a particle and track it until it changes to a different coordination value. Until that event, the particle is considered as a survivor. The number of survivors are counted in each frame, yielding a time series of counts that serves as our survival function. To avoid systematic errors caused by particles moving outside the camera’s field of view (FOV), we track only those within a central region comprising 83% of the FOV at the starting time.

We prepare survival functions for four conditions: non-defects, all defects, five-fold defects, and seven-fold defects. In this way, we quantify how defects and non-defects survive differently, and we differentiate between the survival of five-fold and seven-fold defects. All the steps in this method are illustrated in Fig. 1, where a small sample of data is analyzed to yield four survival functions.

Each experimental run provided a large sample, under steady conditions, with typically 1100 particles that were tracked at each starting time. Each run was so long that we divided it into 40 non-overlapping 1 s time segments, each with its own starting time. We consider each segment as a statistically independent ensemble, allowing us to combine the survival functions for all 40 segments. In the experimental run analyzed in detail in this Rapid Communication, for the 40 starting times combined, there were 30 210 six-fold non-defects, 6982 five-fold defects, and 6910 seven-fold defects. There were also 56 four-fold and 62 eight-fold defects.

*Results.*—Survival functions are presented in Fig. 2. The vertical axis is the fraction of survivors, while the horizontal axis is the time elapsed since the starting time. These results are shown for non-defects in Fig. 2(a), for all defects in Fig. 2(b), and for five-fold and seven-fold defects separately in Fig. 2(c). A single experimental run provided the data in Fig. 2; the other seven runs are presented in the Supplemental Material [55].

Unexpectedly, we find an elbow in the survival-function curve for non-defects. We interpret this feature in the decay as a signature of a microscopic process with dual time-scales. This elbow is seen in Fig. 2(a) at  $t = 200\text{ ms}$ . It is also seen in the other seven experimental runs, giving us confidence in this result.

Defects, on the other hand, have survival-function curves with a shape that is more nearly exponential. This is especially the case for five-fold defects, Fig. 2(c). Seven-fold defects also have a decay that starts exponentially, although at longer times the seven-fold survival curve has a weak but detectable enhancement in its tail. This weak non-exponential feature in the tail for seven-fold defects [and in the tail for all defects combined, Fig. 2(b)], suggests a slight difference in the survival of five and seven-fold defects; explaining this difference would require further study, for example by characterizing departures from pairwise behavior of five and

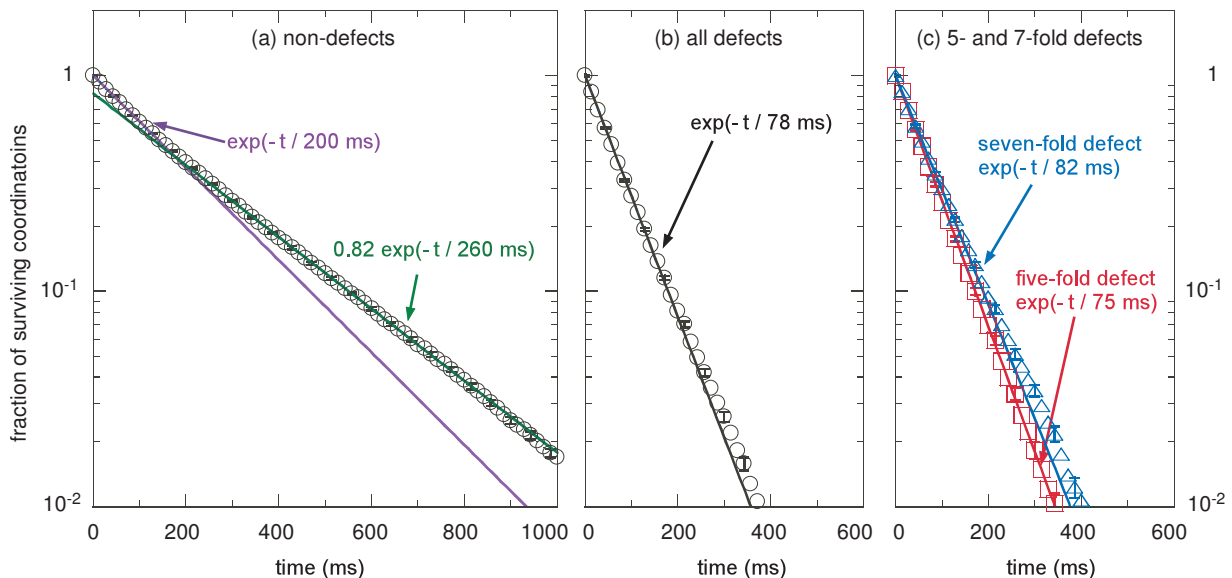


FIG. 2. (color online). Particle-coordination survival functions, obtained with our structural analysis. For non-defects, the curves in (a) have two exponential time scales, revealing a complexity in the microscopic rearrangements. For defects, on the other hand, the survival-function curves in (b) are more nearly exponential. The defect survival function diminishes about three times faster than the survival function for non-defects. Plotting survival functions separately for the common five-fold and seven-fold defects in (c) reveals that they survive differently. Representative error bars due to counting statistics are shown for survivor function data points. Separately, the decay times had uncertainties of  $< 1\%$  from the exponential fits.

seven-fold defects.

As a measure of stability, we now quantify the time scales for the survival-function decay. We do this by fitting the curves in Fig. 2 to exponentials. We expect that non-defects will decay most slowly due to their greater intrinsic stability, and we find that this is indeed so. The exponential times for the dual decay of non-defects are  $200 \text{ ms} = 10.0 \Omega_E^{-1} = 17.2 \omega_{pd}^{-1}$  before the elbow and  $260 \text{ ms} = 13.1 \Omega_E^{-1} = 22.4 \omega_{pd}^{-1}$  after the elbow in Fig. 2(a). Defects decay more rapidly; we find an exponential decay time of  $78 \text{ ms} = 3.9 \Omega_E^{-1} = 6.7 \omega_{pd}^{-1}$  when all defects are considered in aggregate, in Fig. 2(b). Distinguishing the defects, we find that seven-fold defects survive slightly longer than five-fold defects, with an exponential time scale that is about 10% greater, in Fig. 2(c). These decay times for defects diminish with increasing temperature, as shown in the Supplemental Material [55]. The exponential fits for defects are for the data points  $t < 145 \text{ ms}$ , which excludes the slightly enhanced tails.

*Discussion of non-defects.*—The dual time-scale decay exhibited by non-defects in our experiment indicates that their survival must be governed by a behavior more complex than for a simple stochastic system. If survival had just one stochastic process, as in nuclear decay, the survival function would be exactly exponential. Our non-defects have a survival function with an elbow, and this signature of non-stochastic behavior (or multiple stochastic processes), is observed consistently in all our experimental runs [55].

While we cannot yet fully identify the microscopic processes underlying the dual time scales, we have carried out a test that allows us to identify a likely contributing factor: the abundance of defects near a non-defect. As our test, we analyzed data separately for very long-lived and very short-lived non-defects. We found that non-defects that survived a short time had neighborhoods that were richer in defects than for those that survived a long time, likely due to the intrinsic instability of defects. In particular, very short-lived non-defects (those that survived  $< 140 \text{ ms}$ ) had neighborhoods that were  $34 \pm 1\%$  defective, while very long-lived non-defects (those that survived  $> 714 \text{ ms}$ ), had neighborhoods that were only  $21 \pm 3\%$  defective [57]. The outcome of this test, that a non-defect's survival depends on its neighborhood, suggests that its survival must be due to processes that include local effects, and not just effects with homogenous probabilities.

*Discussion of defects.*—Although the literature for 2D liquids generally relies on the idea that defects are eliminated as five-seven pairs [58], we find that this not entirely the case. A signature of pairwise elimination would be survival-function curves that diminishes identically for five- and seven-fold defects. However, these two curves have detectable differences in our experimental data: the decay for five-fold defects is faster and more precisely exponential than for seven-fold defects. Detecting such a difference might be more difficult if one relied on a visual inspection of defect maps instead of a survival-function analysis.

*Summary.*— We uncovered a complexity in the way a liquid gradually forgets its local microscopic structure. Unexpectedly, two distinct time scales were found for the conversion of non-defects into defects. The survival of defects, on the other hand, has a simpler and faster decay, which is nearly exponential and varies with temperature and the type of defect.

Our findings for relaxation in a liquid were made possible by a new analysis method, in which particle coordination data are distilled not into a single time-scale parameter, but into survival functions. These survival functions are time-series graphs of the number of particles that have a coordination that has remained unchanged. Survival-function analysis could be used also for other liquid-like systems, including molecular-dynamics simulations, colloidal experiments [59], and foams.

This work was supported by the US National Science Foundation Award 1162645, US Department of Energy Grant DE-SC0014566, and NASA Subcontract 1562068.

---

\* Present address: Sandia National Laboratories, Livermore, CA 94550, USA; tim.cs.wong@gmail.com

† Present address: Lockheed Martin Aeronautics, Palm-dale, CA 93599, USA

- [1] S. Ichimaru, *Rev. Mod. Phys.* **54**, 1017-1059 (1982).
- [2] K. I. Golden and G. J. Kalman, *Phys. Plasmas* **7**, 14 (2000).
- [3] M. S. Murillo, *Phys. Plasmas* **11**, 2964 (2004).
- [4] V. E. Fortov, I. T. Iakubov, and A. G. Khrapak, *Physics of Strongly Coupled Plasma* (Clarendon Press, Oxford, 2006).
- [5] H. Kählert, G. J. Kalman, and M. Bonitz, *Phys. Rev. E* **90**, 011101 (2014).
- [6] C.-S. Wong, J. Goree, Z. Haralson, and B. Liu, *Nat. Phys.* **14**, 21-24 (2018).
- [7] V. E. Fortov, A. P. Nefedov, O. F. Petrov, A. A. Samarian, and A. V. Chernyshev, *Phys. Rev. E* **54**, R2236-R2239 (1996).
- [8] R. L. Merlino and J. A. Goree, *Phys. Today* **57**, No. 7, 32 (2004).
- [9] M. Bonitz, C. Henning, and D. Block, *Rep. Prog. Phys.* **73**, 066501 (2010).j
- [10] V. E. Fortov, A. V. Ivlev, S. A. Khrapak, A. G. Khrapak, and G. E. Morfill, *Phys. Rep.* **421**, 1 (2005).
- [11] S. V. Vladimirov, K. Ostrikov, and A. A. Samarian, *Physics and Applications of Complex Plasmas* (Imperial College Press, London, 2005).
- [12] P. M. Bellan, *Fundamentals of Plasma Physics* (Cambridge University Press, Cambridge, 2006), Chap. 17.
- [13] A. Piel, *Plasma Physics: An Introduction to Laboratory, Space, and Fusion Plasmas* (Springer-Verlag, Berlin, 2010), Chap. 10.
- [14] C. Killer, T. Bockwoldt, S. Schutt, M. Himpel, A. Melzer, and A. Piel, *Phys. Rev. Lett.* **116**, 115002 (2016).
- [15] Y.-Y. Tsai, J.-Y. Tsai, and L. I, *Nat. Phys.* **12**, 573-577 (2016).
- [16] G. Gogia and J. C. Burton, *Phys. Rev. Lett.* **119**, 178004 (2017).
- [17] Z. Haralson and J. Goree, *IEEE Trans. Plasma Sci.* **44**, 549-552 (2015).
- [18] Y. Feng, J. Goree, and B. Liu, *Rev. Sci. Instrum.* **78**, 053704 (2007).
- [19] Y. Feng, J. Goree, and B. Liu, *Rev. Sci. Instrum.* **82**, 053707 (2011).
- [20] P. K. Kaw and A. Sen, *Phys. Plasmas* **5**, 3552 (1998).
- [21] M. S. Murillo, *Phys. Rev. Lett.* **85**, 2514-2517 (2000).
- [22] B. S. Xie and M. Y. Yu, *Phys. Rev. E* **62**, 8501-8507 (2000).
- [23] P. Hartmann, M. C. Sándor, A. Kovács, and Z. Donkó, *Phys. Rev. E* **84**, 016404 (2011).
- [24] J. Goree, Z. Donkó, and P. Hartmann, *Phys. Rev. E* **85**, 066401 (2012).
- [25] G. Bannasch, J. Castro, P. McQuillen, T. Pohl, and T. C. Killian, *Phys. Rev. Lett.* **109**, 185008 (2012).
- [26] A. Gupta, R. Ganesh, and A. Joy, *Phys. Plasmas* **21**, 073707 (2014).
- [27] J. Ashwin and A. Sen, *Phys. Rev. Lett.* **114**, 055002 (2015).
- [28] A. Diaw and M. S. Murillo, *Phys. Rev. E* **92**, 013107 (2015).
- [29] T. S. Strickler, T. K. Langin, P. McQuillen, J. Daligault, and T. C. Killian, *Phys. Rev. X* **6**, 021021 (2016).
- [30] Z. Haralson, J. Goree, and R. Belousov, *Phys. Rev. E* **98**, 023201 (2018).
- [31] J. C. Maxwell, *Philos. Trans. R. Soc.* **157**, 49-88 (1867).
- [32] Survival functions have different names in various fields; these include: survivor function, reliability function, and activity plot.
- [33] D. Kleinbaum and M. Klein, *Survival Analysis: A Self-Learning Text*, 2nd ed. (Springer Science+Business Media, Inc., New York, 2005).
- [34] T. G. Clark, M. J. Bradburn, S. B. Love, and D. G. Altman, *Br. J. Cancer* **89**, 232-238 (2003).
- [35] A. Birolini, *Reliability Engineering: Theory and Practice*, 7th ed. (Springer-Verlag, Berlin Heidelberg, 2014).
- [36] B. M. Weon and J. H. Je, *Sci. Rep.* **2**, 504 (2012).
- [37] C. Murray and D. Grier, *Annu. Rev. Phys. Chem.* **47**, 421-462 (1996).
- [38] J.-P. Hansen and I. R. McDonald, *Theory of Simple Liquids*, 2nd ed. (Academic Press, New York, 1986).
- [39] A. K. Soper and M. A. Ricci, *Phys. Rev. Lett.* **84**, 2881-2884 (2000).
- [40] P. Wernet, D. Nordlund, U. Bergmann, M. Cavalleri, M. Odelius, H. Ogasawara, L. Näslund, T. K. Hirsch, L. Ojamäe, P. Glatzel *et al.*, *Science* **304**, 995 (2004).
- [41] T. Iwashita and T. Egami, *Phys. Rev. Lett.* **108**, 196001 (2012).
- [42] T. Iwashita, D. M. Nicholson, and T. Egami, *Phys. Rev. Lett.* **110**, 205504 (2013).
- [43] Y. Feng, J. Goree, and B. Liu, *Phys. Rev. Lett.* **100**, 205007 (2008).
- [44] W. D. S. Ruhunusiri, J. Goree, Y. Feng, and B. Liu, *Phys. Rev. E* **83**, 066402 (2011).
- [45] Disclination is another term used to describe a non-six-fold coordination.
- [46] Z. Haralson and J. Goree, *Phys. Plasmas* **23**, 093703 (2016).
- [47] Z. Haralson and J. Goree, *Phys. Rev. Lett.* **118**, 195001 (2017).
- [48] H. Ikezi, *Phys. Fluids* **29**, 1764 (1986).
- [49] H. Thomas, G. E. Morfill, V. Demmel, J. Goree, B. Feuerbacher, and D. Möhlmann, *Phys. Rev. Lett.* **73**,

- 652 (1994).
- [50] J. H. Chu and L. I, Phys. Rev. Lett. **72**, 4009 (1994).
- [51] Y. Hayashi and K. Tachibana, Jpn. J. Appl. Phys., Part 2 **33**, L804 (1994).
- [52] A. Melzer, T. Trottenberg, and A. Piel, Phys. Lett. A **191**, 301 (1994).
- [53] C.-S. Wong, J. Goree, and Z. Haralson, IEEE Trans. Plasma Sci. **46**, 763-767 (2018).
- [54] P. Hartmann, A. Douglass, J. C. Reyes, L. S. Matthews, T. W. Hyde, A. Kovács, and Z. Donkó, Phys. Rev. Lett. **105**, 115004 (2010).
- [55] See Supplemental Material at [URL will be inserted by publisher] for a sample video showing how coordinations change in a liquid-like dusty plasma, as well as additional survival function plots for the other experimental runs.
- [56] As a further advantage, for applications beyond the experiment we currently analyze, we note that Delaunay triangulation would avoid erroneous results if the liquid underwent expansion or compression.
- [57] These measures of defect-richness are based on a search radius of about  $2.5a$ , where  $a$  is the Wigner-Seitz radius.
- [58] Elimination of five-seven pairs is often described as occurring through annihilation [X. Sun, Y. Li, Y. Ma, Z. Zhang, Sci. Rep. **6**, 24056 (2016)], which is different from unbinding [D. R. Nelson and B. I. Halperin Phys. Rev. B **19**, 2457-2484 (1979)].
- [59] A. Ivlev, H. Löwen, G. Morfill, and C. P. Royall, *Complex Plasmas and Colloidal Dispersions: Particle-resolved Studies of Classical Liquids and Solids* (World Scientific Publishing Co. Pte. Ltd., Singapore, 2012).